IOP Publishing Journal of Physics A: Mathematical and Theoretical
J. Phys. A: Math. Theor. **53** (2020) 175302 (21pp) https://doi.org/10.1088/1751-8121/ab7d5f

Evolution of superoscillations in a relativistic wavepacket

J R Herklots and P Strange[1]

School of Physical Sciences, University of Kent, Canterbury, Kent, CT2 7NH, United Kingdom

E-mail: P.Strange@kent.ac.uk

Received 20 September 2019, revised 4 March 2020
Accepted for publication 6 March 2020
Published 7 April 2020

Abstract

We analyse the evolution of superoscillations in a relativistic wavepacket. A simple superoscillating wavepacket is set up and is allowed to evolve freely according to both the Klein–Gordon equation and the Dirac equation. The superoscillations evolve anisotropically and decay after a time. Both the lifetime and anisotropy can be understood in terms of the interaction of contributions to the wavepacket from components with strongly differing complex wavenumber. The analysis is supported by numerical calculations and the results are compared with the non-relativistic analysis. A potential experiment in which the significance of relativistic effects on superoscillations could be measured is proposed.

Keywords: superoscillations, Klein–Gordon equation, Dirac equation

(Some figures may appear in colour only in the online journal)

1. Introduction

A superoscillating function is a band-limited function that oscillates faster than its fastest Fourier component. A few decades ago, this would have been deemed impossible, such a statement initially seems paradoxical. However, such functions have been known for decades [1], but their remarkable properties only began to be realised in the late 1980's [2] and they have only been studied systematically since the mid-1990's [3]. Superoscillations are now well understood [4–14] both mathematically and physically.

Superoscillations gained the attention of experimentalists when it was also predicted that superoscillating wavepackets could be employed to image objects in sub-wavelength detail [15, 16] and there are now some impressive applications in sub-wavelength microscopy [17–19] and radar [1]. Superoscillations have even been found in a single photon [20]. The 'state of the

[1] Author to whom any correspondence should be addressed.

art' in our understanding of the mathematical aspects of superoscillations and their burgeoning number of applications is provided by Berry *et al* [21] and Chen *et al* [22].

In quantum mechanics Berry and Popescu [23] showed how a superoscillatory function evolves according to the free-particle Schrödinger equation. Using a prototypical superoscillatory wavepacket as the initial wavefunction, it was found that the superoscillations persist for a far longer time than expected—noticeably longer than exponentially decaying evanescent waves. This behaviour was explained through the interaction of contributions to the wavefunction appearing as complex momenta in the phase. It is this persistence of superoscillations that has been of most interest in the area of quantum superoscillations with the case of the harmonic oscillator [24, 25], a uniform electric field [14] and a uniform magnetic field [26] all being studied. In these cases it is found that superoscillations behave in much the same way as they do for free particles, although in the harmonic oscillator potential they re-form periodically. For the case of the electric field, it is found that the superoscillations disappear on a time scale identical to that of the free-particle. However, in this interpretation and others [14] a more general Hamiltonian was used and, consequently, it was found that the time for which superoscillations exist is dependent on the initial wavevector (actually N in the subsequent theory).

In the end nature is governed by relativistic physics, not non-relativistic physics and these previous studies all contain the inherent approximation of being non-relativistic. While this is true of all non-relativistic theory, in the case of superoscillations it is particularly salient because they are exponentially small and relativistic effects may well be of the same order of magnitude as the superoscillations themselves. Any experimental predictions or physical applications based on the work of Berry and Popescu have an unknown limitation for this reason. In the present paper we remove this approximation to address the question of how relativity affects the formation, behaviour and decay of superoscillations within quantum theory. In principle this deepens our understanding of the subject and provides a more realistic understanding of the theoretical limits of many of the above applications.

One way in which superoscillations can be probed was suggested by Berry and Popescu [23]. Because their wavefunction $\psi(x)$ is periodic it can represent a grating that transforms an incident plane of quantum particles into a propagating series of diffracted beams. For incident light such a grating could be manufactured by programming a spatial light modulator. If the relativistic theory can be fully understood and an analogous 'grating' can be manufactured for particles it could be used to create particle beams which can be used to measure relativistic effects on superoscillations directly. These beams will also have unusual cross sectional profiles for further experiments and applications. We examine how superoscillations evolve in relativistic single particle quantum mechanics by considering in detail a simple superoscillating wavepacket and comparing our results with those derived from the Schrödinger equation. There is no reason to believe that the wave packet we have chosen is not typical of any superoscillating wavepacket.

The paper is laid out as follows. In the following section we introduce and discuss the elementary properties of our wavepacket. Then in section 3 we discuss an initial wave packet of this form that is allowed to evolve as a relativistic spin-0 particle according to the Klein–Gordon equation. In the following section we examine the evolution for a spin-1/2 particle and show that if the Dirac equation is written in a convenient representation the solutions of the Klein–Gordon equation can be used to deduce the behaviour of all components of the Dirac wavefunction. Finally we compare the results from both relativistic wave packets and draw some conclusions about relativistic effects on superoscillating behaviour. Because they are rarely discussed we also provide an appendix discussing relativistic first quantised propagators.

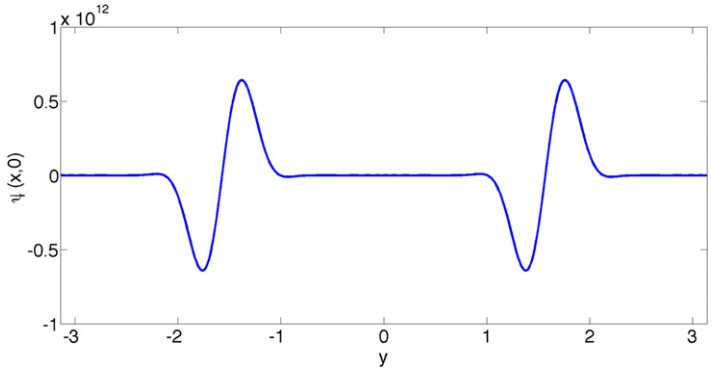

Figure 1. The wavepacket described by equation (1) for $\mathcal{N} = 20$, $a = 4$ and $k = 1$. The flat region centred on the origin is where the superoscillations exist.

2. Superoscillations

Following Berry and Popescu we consider the wavepacket

$$\psi(x, 0) = (\cos(x) + \mathrm{i}a\ \sin(x))^{\mathcal{N}} \tag{1}$$

where $a > 1$ is a number, and $\mathcal{N}$ is large. $\psi(x, 0)$ is a repeating function with period 2π. Obviously for $a = 1$ it is a simple plane wave. The properties of this wavepacket have been considered in detail by Aharonov and co-workers [4]. Close to $x = 0$ we can write $\psi(x, 0)$ as

$$\psi(x, 0) = \exp(\mathcal{N}\ \log(1 + \mathrm{i}ax)) \approx \exp(\mathrm{i}a\mathcal{N}x) \tag{2}$$

which is a simple plane wave with effective wave vector $a\mathcal{N}$. In [23] Berry and Popescu evaluated the Fourier series for $\psi(x, 0)$ and found

$$\psi(x, 0) = \sum_{n=0}^{\mathcal{N}} c_n\ \exp(\mathrm{i}\mathcal{N}\kappa_n x) \tag{3}$$

with

$$\kappa_n = 1 - \frac{2n}{\mathcal{N}} c_n = (-1)^n \frac{(\mathcal{N})!}{2^{\mathcal{N}}} \frac{(a^2 - 1)^{\mathcal{N}/2}}{[\mathcal{N}(1 + \kappa_n)/2]![\mathcal{N}(1 - \kappa_n)/2]!} \left(\frac{a - 1}{a + 1}\right)^{\mathcal{N}\kappa_n/2} \tag{4}$$

which is band-limited, containing only wavenumbers $|\kappa_n| \leqslant 1$. Equation (2) can oscillate arbitrarily more rapidly than equation (3) (depending on the value of a) and so this function is described as superoscillating.

In figure 1 we show $\psi(x, 0)$ for $\mathcal{N} = 20$ and $a = 4$. The superoscillations occur close to $x = 0$ where the wavepacket is flat in this figure. This is representative of a general property of superoscillating wavepackets. Superoscillations occur in regions of space where the amplitude

of the wave is exponentially small. The question that then arises is how to display superoscillations in a way that enables them to be observed. We do this by plotting the logarithm of the real part of the wavepacket, the imaginary part behaves similarly. Then, because $\log 0 = -\infty$, the nodes of the wavefunction are easily seen.

3. Spin-0 wavepackets

3.1. The Klein–Gordon equation

In relativistic quantum theory spin-zero particles are described by the Klein–Gordon equation [27] and it is this case we focus upon. We will consider free particles in $1+1$ dimensions only and this equation then takes the form

$$\left(-\frac{1}{c^2}\frac{\partial^2}{\partial t^2}+\frac{\partial^2}{\partial x^2}\right)\psi(x,t)=N^2c^2\psi(x,t). \tag{5}$$

In general the solutions to this can be written in terms of plane waves

$$\psi(x,t)=\sum_n A_n\ \exp(\mathrm{i}(k_n x-\omega_n t)) \tag{6}$$

with

$$\omega_n^2=k_n^2c^2+N^2c^4. \tag{7}$$

In these equations we have replaced $m/\hbar$ by N in the usual form of the Klein–Gordon equation. This is convenient because later on Nc will be assumed to be large. We can take the linear combination in equation (6) corresponding to the wavepacket of equation (1) at $t=0$. That means we identify A_n with c_n, $k_n=\mathcal{N}\kappa_n$ and $\mathcal{N}=Ncs$ where s is a constant with spatial dimensions and magnitude $1/c$, which is required for the dimensions to make sense. It will be seen later that s does have a significant role to play in the evolution of superoscillations in this wavepacket. It is then clear that the solutions at all times are

$$\psi(x,t)=\sum_{m=0}^{N} c_n\ \exp(\mathrm{i}Ncsk_nx-\omega_n t) \tag{8}$$

$$\omega_n^2=N^2k_n^2s^2c^4+N^2c^4 \tag{9}$$

In figure 2 we display the superoscillations as a function of position for a series of increasing times. Figure 2(a) is for $t=0$ and shows the superoscillations in the central region of figure 1. The graphs in figure 2 have been evaluated at the same times as those in figure 4 of reference [23]. Comparison of their figure with ours shows that the figures are broadly similar, but differ substantially in detail. In particular we note that the figures rapidly lose their symmetry. In figures 2(c) and (d) for example, the wavepacket hardly passes through zero at all for $x<0$ while it does so frequently for $x>0$. This suppression of superoscillations on one side of the origin was termed 'the wall effect' by Berry and Popescu [7]. We can also see from this figure that by time $t=\pi/2$ the super oscillations have disappeared. To better view the evolution of superoscillations and see the effects of relativity we plot a space–time map of the density $\log(\Re(\psi(x,t)))$ in figure 3. In this figure we have removed the rest mass frequency Nc^2 from ω to make direct comparison with the non-relativistic case. It

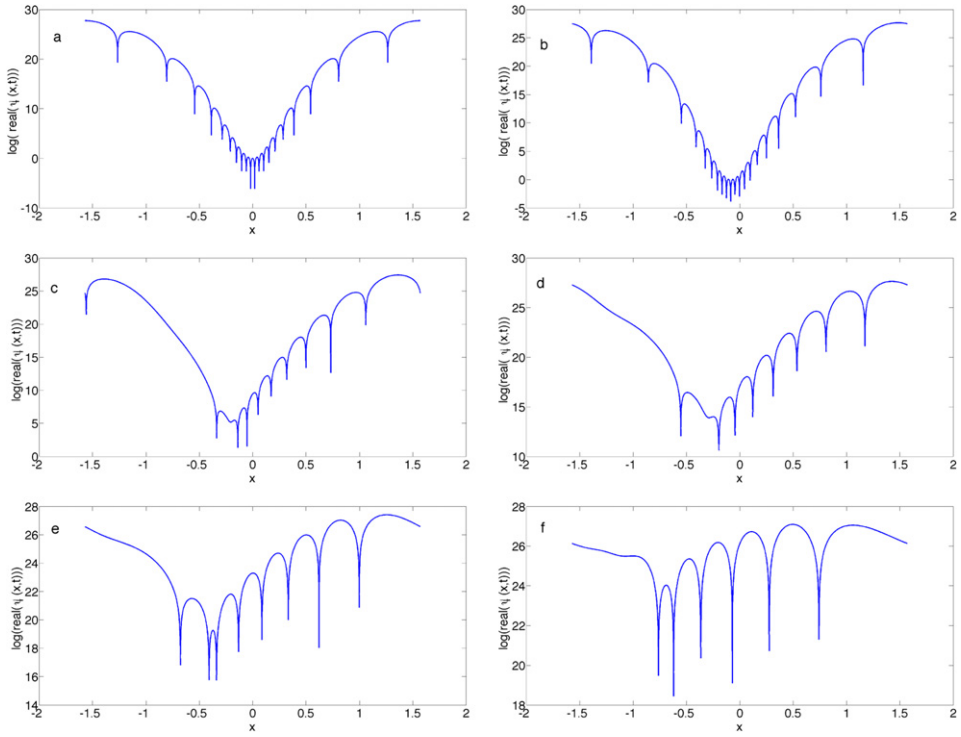

Figure 2. The logarithm of the real part of the wavepacket described by equation (8) for $\mathcal{N} = 20$, $a = 4$ and $c = 2$ at a series of times: (a) $t = 0$; (b) $t = 0.015\pi$; (c) $t = 0.08\pi$; (d) $t = 0.706$; (e) $t = \pi/2$; (f) $t = \pi$.

should be noted that the white lines (the wavefunction zeroes) are the only physically significant quantity on these figures. The greyscale has a normalisation dependence which is not necessarily identical in each figure. Figures 3(a) and (b) show the non-relativistic limit of our code taken by setting $c = 50$ and presented on two different scales. Comparison with figure 3 of the paper by Berry and Popescu shows that the lines are identical apart from an unimportant inversion about $x = 0$ which we cannot explain. There is an apparent rescaling, but this is simply due to the relativistic units we have employed. Figures 3(c) and (d) show the superoscillations when we emphasise relativistic effects more by setting $c = 2$ and figures 3(d) and (e) are for when $c = 1$. In this paper we wish to emphasise relativistic effects and the usual way to do this would be to set $c = 1$. If we do that in this case the kinetic energy of the highest Fourier component is equal to Nc^2 and we would have to consider particle/antiparticle creation. Therefore we have set $c = 2$ throughout the rest of this paper which means the kinetic energy is still a large fraction of the rest mass energy, but well below it, so we can ignore particle/antiparticle creation and the one-particle approach is an excellent approximation.

Displaying superoscillations using the logarithm of the real part of the wavefunction means we are displaying its phase. Subtracting the rest mass energy changes the phase and so our results depend on this. To display this explicitly we present figure 4 where we show the evolution of superoscillations for when the rest mass energy is removed from the total and the full relativistic case where it is included. Clearly the results are very different and figure 4(a) is the

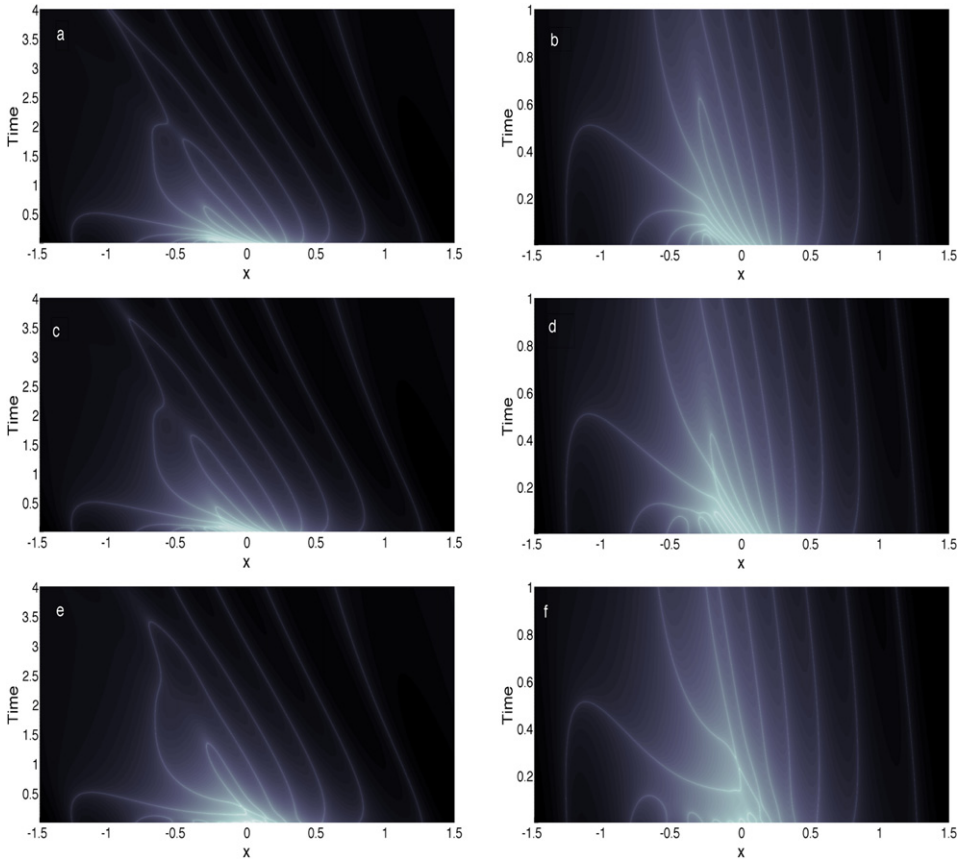

Figure 3. Density maps for log $\Re(\psi(x,t))$ on a large (left column) and more detailed (right column) scale for a wavepacket with $a = 4$ and $N = 20$. (a) and (b) for $c = 50$ (the non-relativistic limit), (c) and (d) for $c = 2$ (the relativistic case), (e) and (f) for $c = 1$ (the strongly relativistic case).

correct one to compare with the non-relativistic limit while figure 4(b) is the one that is more correct within a fully relativistic theory. Henceforth we will display superoscillations with the full relativistic energy.

While figures 3 and 4 are informative we can gain little insight into the reasons for the wall effect and the disappearance of super oscillations from them. To make further progress we examine the wavefunction as a function of time using a propagator approach.

3.2. Quantum evolution in terms of the relativistic propagator

The Klein–Gordon propagator is derived in the appendix. To gain a deeper understanding we write the wavefunction in the propagator representation

$$\begin{aligned}\psi(x,t) &= \int_{-\infty}^{\infty} \psi(x',0) \triangle (x-x',t)\mathrm{d}x' \\ &= \frac{A}{\sqrt{L}}\frac{\mathrm{i}N}{\pi}c^2 t\int_{-\infty}^{\infty}(\cos kx' + \mathrm{i}a\,\sin kx')^{Ncs}\frac{K_1\left(Nc\sqrt{(x-x')^2-c^2t^2}\right)}{\sqrt{(x-x')^2-c^2t^2}}\mathrm{d}x' \qquad (10)\end{aligned}$$

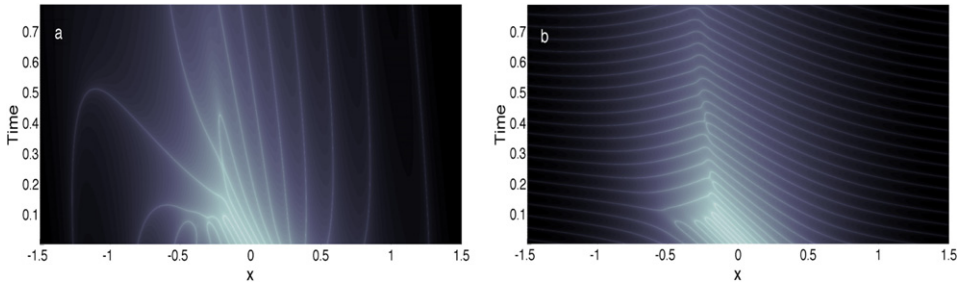

Figure 4. Density maps for log $\Re(\psi(x,t))$ for a wavepacket with $a = 4$ and $N = 20$. (a) Calculated with the rest mass subtracted from the total relativistic energy; (b) calculated with the full relativistic energy.

where A is the normalisation constant and L is the normalisation length. We have also introduced a simple wave vector k to give us control over the scale of the problem and to simplify the units. The integrand here is a complex function containing saddle points plus poles at $x' = x \pm ct$. We now consider evaluating this integral at various levels of approximation.

3.2.1. The poles. To take account of the contribution to the integral from the poles at $x' = x \pm ct$ we make the light cone approximation to the propagator. This is given by equation (28). Putting this into equation (10), separating into partial fractions and retaining only positive times yields

$$\begin{aligned}\psi(x,t) &= -\frac{\mathrm{i}A}{2\pi\sqrt{L}}\int_{-\infty}^{\infty}\frac{(\cos kx' + \mathrm{i}a\,\sin kx')^{Ncs}}{x - x' + ct}\mathrm{d}x' \\ &= -\frac{\mathrm{i}A}{2\pi\sqrt{L}}\sum_{m=0}^{Ncs} c_m \int_{-\infty}^{\infty}\frac{\mathrm{e}^{\mathrm{i}Ncsk_m x'}}{x - x' + ct}\mathrm{d}x' \end{aligned} \tag{11}$$

where in the final step we have replaced the explicit form of the wavepacket by its Fourier decomposition. This integral can be evaluated using the residue theorem. However care must be taken when deforming the contour. The terms with negative k_m diverge as $x' \to +\mathrm{i}\infty$ and the terms with positive k_m diverge as $x' \to -\mathrm{i}\infty$. When $k_m = 0$ the integral is convergent and which contour is selected does not matter. The contours chosen are shown in figure 5. Taking all this into account a trivial calculation then yields

$$\psi(x,t) = \frac{A}{\sqrt{L}}(\cos(k(x+ct)) + \mathrm{i}a\,\sin(k(x+ct)))^{Ncs} \tag{12}$$

This turns out to be a very poor approximation to the full wavefunction after $t = 0$ and cannot tell us anything about superoscillations. This is because the light cone approximation propagates the initial wavefunction at the speed of light whereas the actual evolution involves the interference of $2N + 1$ plane waves all travelling at different speeds.

3.2.2. The saddle points. In order to get an expression that is integrable the following representation of the initial wavefunction is used

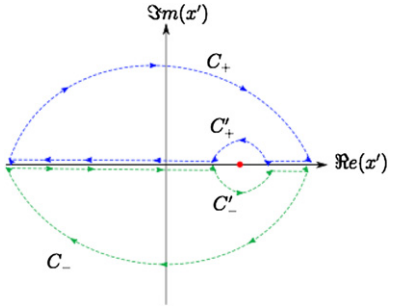

Figure 5. This figure shows how the sign of k_m in equation (11) affects how the contour is deformed around the pole (red circle) at $x' = x + ct$ in the x' plane. If $k_m > 0$ the contour is deformed to C_+ and if $k_m < 0$ it is deformed to C_-.

$$\psi(x,0) = \frac{A}{\sqrt{L}}(\cos\ kx + \mathrm{i}a\ \sin\ kx)^{Ncs} = \frac{A}{\sqrt{L}}\exp\left[\mathrm{i}Ncs\int_0^x q(x'')\mathrm{d}x''\right] \tag{13}$$

where $q(x)$ is an effective local complex wavevector (momentum) given by

$$q(x) = -\mathrm{i}\frac{\partial}{\partial x}\log\ (\cos\ kx + \mathrm{i}a\ \sin\ kx)] = \frac{ak\ \cos\ kx + \mathrm{i}k\ \sin\ kx}{\cos\ kx + \mathrm{i}a\ \sin\ kx} \tag{14}$$

The wavefunction in this representation is then given by

$$\psi(x,t) = \frac{\mathrm{i}A}{\sqrt{L}}ct\sqrt{\frac{Nc}{2\pi}}\int_{-\infty}^{\infty}\frac{\exp\left(Nc(\mathrm{i}s\int_0^{x'} q(x'')\mathrm{d}x'' - \sqrt{(x-x')^2 - c^2t^2})\right)}{((x-x')^2 - c^2t^2)^{3/4}}\mathrm{d}x' \tag{15}$$

where we have used equation (29) for the propagator. Now Nc can be taken as a large parameter and this integral can, in principle, be done using the saddle point method. The phase of the exponential is defined as

$$\phi(x';x,t) = \mathrm{i}s\int_0^{x'} q(x'')\mathrm{d}x'' - \sqrt{(x-x')^2 - c^2t^2} \tag{16}$$

Differentiating the phase and setting the result equal to zero gives the saddle point condition

$$q(x_j) = \frac{\mathrm{i}(x - x_j)}{s\sqrt{(x-x_j)^2 - c^2t^2}} \tag{17}$$

where x_j are the values of x' at which equation (17) is valid. Interestingly the saddle points occur at values of x' at which the complex wavevector is equal to the derivative of the space–time interval multiplied by i/s. Equation (15) is still not easy to evaluate because the periodic nature of $q(x)$ means there is an infinite number of saddle points. As in the non-relativistic case, super-oscillations occur at low values of x and t so it suffices to make a small x approximation to equations (13) and (14).

$$\begin{aligned}\psi(x,0) &= \frac{A}{\sqrt{L}}(1 + \mathrm{i}akx)^{Ncs}\\ q(x) &= \frac{ak}{1 + \mathrm{i}akx}\end{aligned} \tag{18}$$

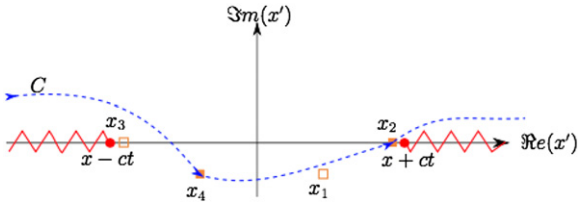

Figure 6. The complex plane in which the integration contour C is deformed through the saddle points at x_2 and x_4.The branch cut emanating from the branch points at $x' = x \pm ct$ is shown in red.

If we substitute this equation for $q(x)$ into equation (17) we obtain a quartic equation for four saddle points. This has been solved this using the *roots* subroutine in Matlab. There are four saddle points two moving forwards in time corresponding to positive energy particles and two moving backwards corresponding to negative energy particles. In order to get a wavefunction of purely positive energy only the saddle points corresponding to time moving forward are considered. It has been found numerically that these are the saddle points at x_2 and x_4 shown in figure 6, and the figure also displays how the contour is deformed to pass through them. Once the saddle points and the contour have been established it is straightforward [29, 30] to find an approximate value of the integral in equation (15).

$$\psi(x,t) \approx \mathrm{i}ct \sum_j \sqrt{\frac{-A}{L\phi''(x_j : x,t)}} \frac{\exp[Nc\phi(x_j;x,t)]}{((x-x_j)^2 - c^2t^2)^{3/4}} \tag{19}$$

where the sum is over contributions from both time-forward saddles. In figure 7 we show the superoscillations not far from $(x,t) = (0,0)$ calculated from equation (19). As explained earlier we plot the superoscillations with the rest mass included in the calculation of the energy in figure 7. Clearly they resemble the exact superoscillations shown in figure 4(b) at low values of x and t but vary from this increasingly as x and t increase. In truth there are small differences even at low values of x and t, but the gross behaviour we wish to examine is still evident. For example in figure 4(b) an approximately vertical line can be discerned where the behaviour of the waves changes. The same line exists, but is less visible in figure 4(a). These lines can also be seen in figure 7, but now move slowly to more positive x as time increases.

At a general point the contribution of the saddles to the total in equation (19) will be exponentially different. There are regions where the x_2 saddle dominates the one at x_4 and vice versa. These regions are separated by anti-Stokes lines where the absolute values of the exponentials in equation (19) are equal. Figure 8 shows the contribution of each saddle point to the total integral in equation (19). We note that there is one discontinuous zero in figure 8(b). This is due to $\phi''(x_j : x,t)$ passing through zero and the saddle point method is invalid close to this point.

If we now compare figure 8 with figure 7 we see that on the left and towards the top of figure 7(a) the superoscillations are dominated by the saddle at x_4 while on the lower right they are dominated by the saddle at x_2. Luckily the place where the saddle point method is invalid for calculating the contribution from x_2 is well inside the regions dominated by the saddle point at x_4 and so it does not affect our discussion. In figure 9 we plot the anti-Stokes line which comes down to close to the origin as $t \to 0$. The discontinuous behaviour along this line is

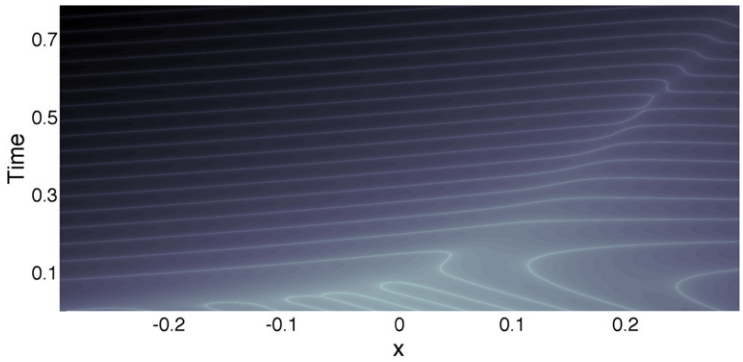

Figure 7. Density maps for log $\Re(\psi(x,t))$ for a wavepacket with $a = 4$ and $N = 20$ calculated using the propagator and the full relativistic energy.

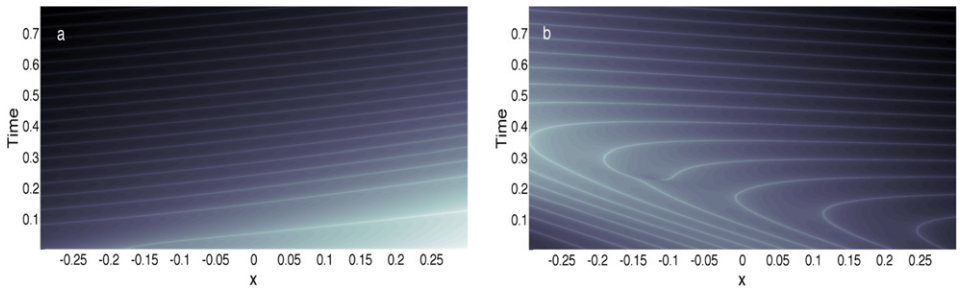

Figure 8. Density maps for log $\Re(\psi(x,t))$ for a wavepacket with $a = 4$ and $N = 20$ calculated using the propagator. (a) Calculated for the saddle at x_4; (b) calculated for the saddle at x_2.

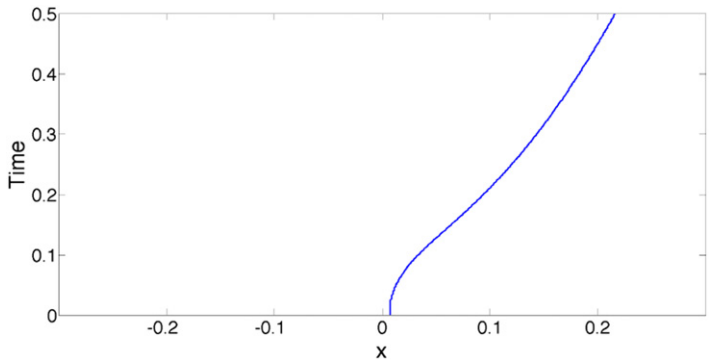

Figure 9. The antiStokes line which divides space into a regions where the wavefunction is dominated by the contribution from the saddle at x_2 (to the right of the antiStokes line) and a region where it is dominated by x_4 (to the left of the antiStokes line).

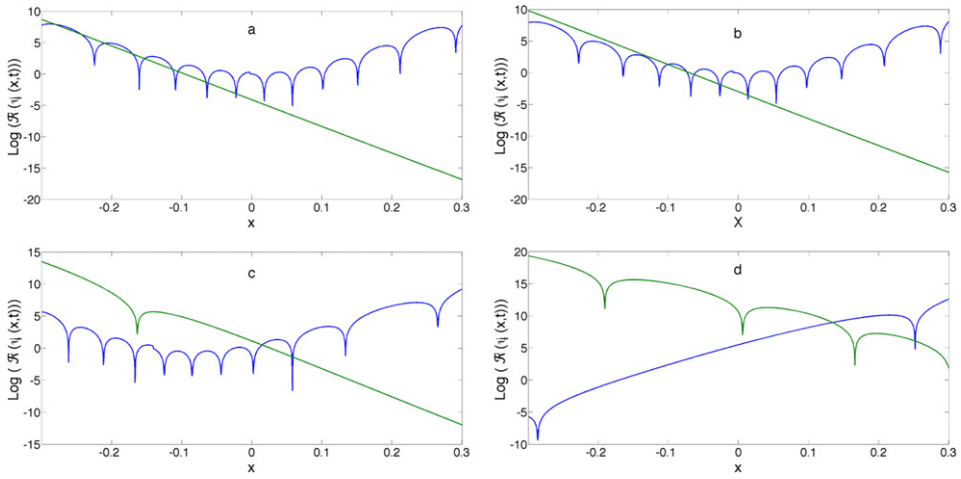

Figure 10. Superoscillations for the relativistic wavefunction of equation (19) blue line contribution from the saddle point at x_2, green line contribution from the saddle point at x_4 at: (a) $t = 0.0005\pi$; (b) $t = 0.0015\pi$; (c) $t = 0.025\pi$; (d) $t = 0.125\pi$.

clearly an exchange of dominance between the two saddles. The superoscillations appear predominantly for $x > 0$ and can definitely be ascribed to the saddle at x_2. For $x < 0$ we initiate the wavefunction with superoscillating behaviour, but this is very quickly suppressed because of the dominance of the saddle at x_4 which does not display superoscillating behaviour. In the region where the superoscillations occur for $x \leqslant 0$ the wave pattern cannot be definitively ascribed to either saddle and the minor factors in equation (19) may be what determines the dominance. To see this we plot the contribution to the total wave from each saddle at particular times in figure 10. At very low times figure 10(a) shows that for $x < 0$ the contributions from both saddles are of the same order and run approximately parallel. However one contribution is superoscillating and the other does not pass through zero in this region. When the contribution from the saddle at x_2 passes through zero the saddle at x_4 dominates and well away from these zeroes the saddle at x_2 dominates. At slightly later times in figure 10(b) the contributions have moved so they are not quite parallel and the region of space where we cannot definitely ascribe dominance to either saddle has reduced. For $x \lesssim -0.15$ the saddle at x_4 dominates while for $x \gtrsim 0$ the saddle at x_2 dominates and leads to superoscillations. For $-0.15 \lesssim x \lesssim 0.0$ neither contribution is dominant and superoscillations will be terminated in this region at around this time. Figure 10 shows a later time where the contribution from the saddle at x_2 is still superoscillating, but below $x = 0$ it is completely dominated by the saddle at x_4 so superoscillations are suppressed in this region. For $x > 0$ it is the saddle at x_2 that dominates, but it does not super oscillate in this region. Finally we see in figure 10(d) a much later time where the superoscillations no longer occur in the saddle at x_2 and the contribution from the saddle at x_4 is oscillating more rapidly. Nonetheless, no superoscillations occur at this time regardless of which saddle point dominates. An interesting point to note is that on close inspection of figures 10(a)–(c) there is a slight discontinuity in the curve due to the saddle point at x_2. This is because the the pole at $x' = x + ct$ interferes with this saddle point, $x_2 \to x + ct$ and $\phi''(x_j : x, t) \to \infty$ and the approximation of treating the saddle and the pole separately becomes incorrect. The effect is surprisingly small. We have used the methods described in the appendix to treat the case where the saddle point and pole coalesce, but that makes no difference to our interpretation of our results, so it is not presented here.

3.3. Analysis

We have calculated the superoscillations for the wavepacket of equation (1) using the propagator and shown that the evolution of the wavepacket is dominated by contributions from two complex saddles. The superoscillations are associated with the saddle point at x_2. It is clear from figures 7, 9 and 10 that there is an anti-Stokes line which marks the exchange in dominance of the two saddles. In general therefore superoscillations occur where the saddle at x_2 is dominant and do not occur where the saddle point at x_4 dominates the wavefunction. Here we present a more quantitative approach to this exchange of dominance. As it happens the saddle point x_4 is more or less constant over the region of small x where our approximations apply. It takes on the value

$$x_4 = -s - \frac{\mathrm{i}}{ak}$$

s was originally introduced simply to make the units consistent in our definition of the regional wavepacket. Now we find it has a crucial role in the theory, being the real part of one of the key saddle points and if we evaluate the wavenumber associated with this saddle it is trivial to see that

$$q_4 = \frac{1}{Ncs}\Re(q(x_4)) = \frac{1}{Ncs}\frac{2ak}{4 + a^2s^2k^2}$$

This means that for our values of the parameters $N = 20$, $a = 4$, $c = 2$ and $k = 1$ the effective wavelength is 40π.(although our approximations are only valid over a small region around $x = 0$).

The saddle point at x_2 is not constant, but can be fit very well with a simple polynomial linear in x and t. While the fit is optimised for this particular values of parameters, computational experiments have shown that the fit is satisfactory over a broad range of these parameters. It also turns out that the anti-Stokes line shown in figure 9 can be fit with a polynomial that is cubic in time and so choosing a value of t enables us to find the associated wavenumber on the anti-Stokes line. At times just greater than $t = 0$ the wavenumber is close to $q_2 = 4$. It decreases rapidly and falls below unity at $t = 0.16$. While these numbers are specific to the wavefunction of equation (1), we expect that an analogous procedure will produce qualitatively similar results for any well-behaved superoscillating wavepacket. Thus we have an understanding of both the wall effect and the life time of the superoscillations.

There are some superoscillations to the left of the anti-Stokes line in figure 9. The reason for this is as follows. As we go from the anti-Stokes line towards $x = -\infty$ at low times the contribution to the wavepacket from both saddles is rising at approximately the same rate. While the contribution from the saddle at x_4 is rising linearly, the contribution from the saddle at x_2 is oscillating rapidly with increasing amplitude. Over a short region of x the minimum in x_2 is more negative than the positive contribution from the x_4 saddle and so the total wavepacket still passes through zero and the superoscillations persist. They have only certainly disappeared when the x_4 contribution is greater than the amplitude of oscillating of the x_2 contribution. So the persistence of the superoscillations to the right of the antiStokes line is a simple two-wave interference effect.

Figure 9 is very different from the corresponding figure of the non-relativistic theory (figure 6 in reference [23]). In the non-relativistic theory there are both Stokes and anti-Stokes lines that are key, as well as a branch cut and a central point from which all these lines emanate. This has not appeared in the relativistic theory. In fact there is a more complex arrangement of such lines in the relativistic theory as well, but they exist relatively far from the origin and so do not affect the superoscillations at all. As $c \to \infty$ the poles move off to $x' \to \pm\infty$ and become

completely irrelevant. Also in this limit the real part of the saddle point $x_4 \to 0$ and then the saddle points can, and do, interfere with each other close to the origin creating a much richer structure of Stokes and anti-Stokes lines in the regions close to where the superoscillations occur.

4. Spin-1/2 wavepackets

4.1. The Dirac equation

The fundamental equation of relativistic quantum theory is the Dirac equation

$$\left(\mathrm{i}\gamma^{\mu}\partial_{\mu} - Nc\right)\psi\left(\mathbf{r},t\right) = 0 \tag{20}$$

Here we have defined $N = m/\hbar$. The 4×4 γ-matrices can be chosen for convenience provided they obey well known anticommutation relations [27]. We choose the representation suggested in reference [33]

$$\gamma^0 = \begin{pmatrix} 0 & I \\ I & 0 \end{pmatrix} \gamma^i = \begin{pmatrix} 0 & -\sigma^i \\ \sigma^i & 0 \end{pmatrix} \tag{21}$$

Here I is the 2×2 identity matrix and σ^i are the standard Pauli spin matrices. The wavefunction is a four component quantity $(\psi_1(\mathbf{r},t), \psi_2(\mathbf{r},t), \psi_3(\mathbf{r},t), \psi_4(\mathbf{r},t))^{\mathrm{T}}$. Putting these into equation (20) gives

$$\begin{aligned}
\psi_1(\mathbf{r},t) &= -\frac{\mathrm{i}}{Nc}\left[\left(\frac{1}{c}\frac{\partial}{\partial t} + \frac{\partial}{\partial z}\right)\psi_3(\mathbf{r},t) + \left(\frac{\partial}{\partial x} - \mathrm{i}\frac{\partial}{\partial y}\right)\psi_4(\mathbf{r},t)\right] \\
\psi_2(\mathbf{r},t) &= -\frac{\mathrm{i}}{Nc}\left[\left(\frac{1}{c}\frac{\partial}{\partial t} - \frac{\partial}{\partial z}\right)\psi_4(\mathbf{r},t) + \left(\frac{\partial}{\partial x} + \mathrm{i}\frac{\partial}{\partial y}\right)\psi_3(\mathbf{r},t)\right] \\
\psi_3(\mathbf{r},t) &= -\frac{\mathrm{i}}{Nc}\left[\left(\frac{1}{c}\frac{\partial}{\partial t} - \frac{\partial}{\partial z}\right)\psi_1(\mathbf{r},t) - \left(\frac{\partial}{\partial x} - \mathrm{i}\frac{\partial}{\partial y}\right)\psi_2(\mathbf{r},t)\right] \\
\psi_4(\mathbf{r},t) &= -\frac{\mathrm{i}}{Nc}\left[\left(\frac{1}{c}\frac{\partial}{\partial t} + \frac{\partial}{\partial z}\right)\psi_2(\mathbf{r},t) - \left(\frac{\partial}{\partial x} + \mathrm{i}\frac{\partial}{\partial y}\right)\psi_1(\mathbf{r},t)\right]
\end{aligned} \tag{22}$$

These equations define the relations between the different components of the Dirac wavefunction. It is well-known that if we eliminate components between them each individual component obeys the Klein–Gordon equation. We will make use of this fact in what follows.

Now we are going to specialise down to $1 + 1$ dimensions. Firstly let us consider motion confined to the z-axis. Then these equations become

$$\begin{aligned}
\psi_1(z,t) &= -\frac{\mathrm{i}}{Nc}\left(\frac{1}{c}\frac{\partial}{\partial t} + \frac{\partial}{\partial z}\right)\psi_3(z,t) \\
\psi_2(z,t) &= -\frac{\mathrm{i}}{Nc}\left(\frac{1}{c}\frac{\partial}{\partial t} - \frac{\partial}{\partial z}\right)\psi_4(z,t) \\
\psi_3(z,t) &= -\frac{\mathrm{i}}{Nc}\left(\frac{1}{c}\frac{\partial}{\partial t} - \frac{\partial}{\partial z}\right)\psi_1(z,t) \\
\psi_4(z,t) &= -\frac{\mathrm{i}}{Nc}\left(\frac{1}{c}\frac{\partial}{\partial t} + \frac{\partial}{\partial z}\right)\psi_2(z,t)
\end{aligned} \tag{23}$$

As expected the Dirac equation has separated into two identical pairs, one pair representing a spin up particle and the other pair a spin down particle. This tells us that superoscillations in a spin-up particle will be identical to those in a spin-down particle. As these equations are identical we need only consider one of them.

Let us look at what happens if we consider motion confined to the x-axis. To proceed we are going to set $\psi_2(\mathbf{r}, t) = 0$. This means we do not have the most general solution of the Dirac equation. Putting this into the equations for $\psi_3(\mathbf{r}, t)$ and $\psi_4(\mathbf{r}, t)$ and substituting these back into the expression for $\psi_2(\mathbf{r}, t)$ gives zero identically, so this procedure is valid. In that case

$$\begin{aligned}\psi_1(x,t) &= -\frac{\mathrm{i}}{Nc}\left(\frac{1}{c}\frac{\partial\psi_3(x,,t)}{\partial t} + \frac{\partial\psi_4(x,t)}{\partial x}\right)\\ \psi_3(x,t) &= -\frac{\mathrm{i}}{Nc^2}\frac{\partial\psi_1(x,t)}{\partial t}\\ \psi_4(x,t) &= \frac{\mathrm{i}}{Nc}\frac{\partial\psi_1(x,t)}{\partial x}\end{aligned} \tag{24}$$

With these limitations we can also put the expressions for $\psi_3(x, t)$ and $\psi_4(x, t)$ into the expression for $\psi_1(x, t)$ to obtain the Klein–Gordon equation (5) [27, 34] for $\psi_1(x, t)$ as expected. Now it is easy to find the solution of the Dirac equation for these cases. For motion in the z-direction we take a solution of the one-dimensional Klein–Gordon equation and differentiate it with respect to z and time to determine $\psi_3(z, t)$ in equation (23). For motion in the x-direction we also take a solution of the one-dimensional Klein–Gordon equation and differentiate it with respect to t and x to determine $\psi_3(x, t)$ and $\psi_4(x, t)$ respectively in equation (24).

The procedure required to investigate superoscillations in a Dirac wavepacket is now clear. $\psi_1(\mathbf{r}, t)$ is set up as a solution of the Klein–Gordon equation starting from the initial wavefunction of equation (1) in its representation as a Fourier series. Then we can use the procedure above to find the other components of the wavefunction. We have done this and the results are shown in figure 11. Figure 11(a) shows the large component of the wavefunction. By construction this is identical to the superoscillations in the Klein–Gordon equation shown in figure 4(b). It is independent of the direction of motion. In figure 11(b) we see the superoscillations in the small component of the wavepacket assuming the momentum is parallel to the spin, i.e. the small component is calculated using the third of equation (23). Figures 11(c) and (d) show the superoscillations in the small components of the wavepacket assuming the spin is perpendicular to the momentum. These are deduced from the third and fourth of equation (24).

4.2. Analysis

The large component of the wavefunction is a solution of the Klein–Gordon equation and the superoscillations shown in figure 11(a) have the same origin as previously. It is well described by equation (19) which describes the full wavefunction as a sum of contributions from two saddle points. The superoscillations evolve from the saddle point at x_2. The wall effect originates from the exchange of dominance between the two saddle points as described earlier. The anti-Stokes line separating these two regions is clearly visible. We can carry this description of $\psi_1(\mathbf{r}, t)$ through to equations (23) and (24) and differentiate the contribution from each saddle point separately, then add them to get the full contribution for each small component of

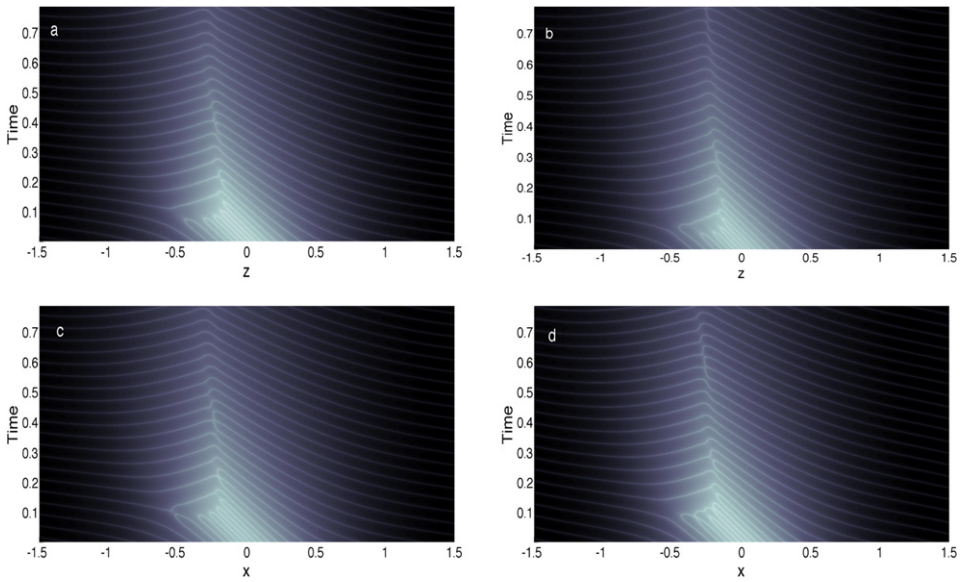

Figure 11. Space time map of superoscillations from the Dirac equation. (a) In $\psi_1(\mathbf{r}, t)$, the large component of the wavefunction. This is independent of whether the motion is in the x or z directions; (b) in $\psi_3(z, t)$, the small component of the wavepacket when the momentum is parallel to the spin. (c) $\psi_3(x, t)$, one of the small components of the wave-packet when the momentum is perpendicular to the spin; and (d) in $\psi_4(x, t)$, the extra small component of the wavefunction when the momentum is perpendicular to the spin.

the wave-packet. If we do this the separate regions where the saddle points dominate and the anti-Stokes line should remain the same and indeed in figures 11(b)–(d) this is apparent. The general solution of the Klein–Gordon equation is given by equation (6) and to obtain the other components of the solution of the Dirac equation in this representation only requires some differentiations (that was the reason for this particular choice of the gamma-matrices) which do not change the exponentials in the wave-packet, so the saddle points will be the same for all components of the wavefunction. This means we will also observe the same wall effect and lifetime.

The superoscillations in the Dirac case are essentially unobservable because they are exponentially small and because when one component of the wavefunction passes through zero the other components cannot be zero and that means the probability density is always greater than zero in a single particle theory. This means the superoscillations are superimposed on a finite density and cannot be observed using logarithms as done for the individual components of the wave-packet.

5. Conclusions

The Klein–Gordon equation is a relativistic single particle equation representing spin-0 particles. Evolution of an initially superoscillating wavepacket demonstrates that the superoscillations decay and exhibit a wall effect similar to that of the non-relativistic theory [23]. These can be understood in terms of the dominance of different saddle point contributions to the wavepacket. Because of the existence of the negative energy states in relativistic theory the

number of saddle points is four rather than the two of the non-relativistic theory. This means that there is no simple expression for the saddle points as there is in the non-relativistic case and so we are more reliant on numerical work here. Although the arrangement of Stokes and anti-Stokes lines are very different in the region of space–time where superoscillations exist in the non-relativistic and relativistic theories, the decay of superoscillations and the wall effect have the same origin in both cases. There are differences in detail, but in both cases the wall effect and the lifetime of the superoscillations can be understood in terms of the interaction of contributions from different saddle points with strongly differing wavenumbers to the wavepacket. The key difference between the relativistic and non-relativistic theories turns out to be the position of the (nearly) constant saddle point. In the non-relativistic theory it has real part zero and this means there are Stokes lines and a branch cut which all have to be considered because they all lie in the region of space–time in which superoscillations occur. In the relativistic theory this saddle point has been lifted above zero and away from the region where superoscillations occur. Then the Stokes line and branch cut are also not in the superoscillating region of space–time and so need not be considered. This is true for both spin-0 and spin-1/2 wave-packets.

Berry and Popescu [23] pointed out that one way to explore the evolution of superoscillations experimentally could be to exploit the periodicity of $\psi(x)$ as a representation of a diffraction grating. Such a grating will transform incident particles into a series of diffracted beams. They have shown how this occurs and produced density plots of waves beyond the diffraction grating in their figure 8 which show super oscillatory fine structure for light on a scale of $\lambda/4$. They were able to compare the paraxial and exact fields and found substantial differences in detail, but not sufficient to affect their conclusions. The paraxial wave equation is mathematically identical to the Schrödinger equation, so the non-relativistic limit of our work should look identical to the paraxial limit of theirs, and indeed it does. We use their parameters $N = 10$ and $a = 8$ and set $c = 50$ and then we are able to reproduce their figures 8(a) and (c) exactly to the limit of the resolution of their figures. As we reduce c relativistic effects become progressively more emphasised. Therefore a procedure to examine the importance of relativistic effects in superoscillations experimentally would be to do this experiment and then find the optimal value of c to fit the results. Unfortunately, emphasising relativistic effects by decreasing c does not change the scale of superoscillatory behaviour, it remains at about $\lambda/4$. The duration of the superoscillations also remains constant until the strongly relativistic limit when it decreases rapidly. Finally, in common with several other analyses [14, 21, 24–26] we find that the lifetime of the superoscillations in this wavepacket is much the same as that in the non-relativistic case and is, at least approximately, proportional to N.

Appendix. The Klein–Gordon propagator

The properties of first quantised relativistic propagators are rarely discussed. Therefore in this appendix we provide a brief review of their derivations and approximations. We begin by defining $\triangle(x - x', t)$ which propagates the wavefunction at the point $(x', 0)$ through space–time. To represent the evolution of a full wavepacket we have to sum over all initial points to yield

$$\psi(x, t) = \int_{-\infty}^{\infty} \psi(x', 0) \triangle (x'; x, t)\, \mathrm{d}x'$$

which is the familiar integral definition of a propagator. For $t = 0$ we must have $\triangle(x', x, t) = \delta(x')$. It is a standard calculation [28] to show that

$$\triangle_{\pm}(x', x, t) = \pm\frac{\mathrm{i}N}{\pi}c^2 t\frac{K_1\left(Nc\sqrt{(x-x')^2 - c^2t^2}\right.}{\sqrt{(x-x')^2 - c^2t^2}} \tag{25}$$

Here K_1 is a modified Bessel function [31] and we have replaced $m/\hbar$ by N from the standard form of the propagator, because that is more convenient for our purposes. If we plot equation (25) on the complex plane we find that it has poles on the real axis at $x' = x \pm ct$ and an infinite number of saddle points off the real axis. Equation (25) is the closed form of our free Klein–Gordon propagator for positive (+)/negative(−) energy states. Making the substitution $t \to -t$ in the case of the positive energy propagator, gives its negative energy counterpart. This affirms the statement that negative energy wavefunctions are positive energy wavefunctions moving backwards in time. Equation (25) is the starting form used in all our calculations. It has been shown by Thaller [28] that equation (25) can be written in a useful alternative form in different regions of space–time

$$\triangle_{\pm}\left(x'; x, t\right) = \frac{Nc^2t}{2}\begin{cases} \mp\dfrac{H_1^{(2)}\left(Nc\sqrt{c^2t^2 - (x-x')^2}\right)}{\sqrt{c^2t^2 - (x-x')^2}} & (x + ct > x') \\ \dfrac{2\mathrm{i}}{\pi}\dfrac{K_1\left(Nc\sqrt{(x-x')^2 - c^2t^2}\right)}{\sqrt{(x-x')^2 - c^2t^2}} & (|x| + ct < |x'|) \\ \pm\dfrac{H_1^{(1)}\left(Nc\sqrt{c^2t^2 - (x-x')^2}\right)}{\sqrt{c^2t^2 - (x-x')^2}} & (x - ct < x') \end{cases} \tag{26}$$

A. The light cone approximation

If we assume the major contribution to the wavefunction comes from the contribution at the poles of the propagator, equation (25) can be approximated as follows. The argument of the modified Bessel function can be written [31]

$$\lim_{x' \to x \pm ct} K_1(Nc\sqrt{(x-x')^2 - c^2t^2}) \approx \frac{1}{Nc\sqrt{(x-x')^2 - c^2t^2}} \tag{27}$$

leading to

$$\triangle_{\pm}(x'; x, t) = \pm\frac{\mathrm{i}ct}{\pi}((x-x')^2 - c^2t^2)^{-1} \tag{28}$$

Although we have derived this from equation (25) it can also be found from equation (26) coming to the pole from either side.

B. The saddle point approximation

Dealing with only the poles of the propagator may well not be a sufficiently robust approximation. Therefore we consider the contribution of the saddle points to the integral of equation (10). We are working with $N \gg 0$ which means we can approximate the Bessel function in equation (25) using equation (10.25.3) in reference [31] and the propagator becomes

$$\triangle(x'; x, t) \approx \mathrm{i}ct\sqrt{\frac{Nc}{2\pi}}\frac{\exp\left[-Nc\sqrt{(x-x')^2 - c^2t^2}\right]}{((x-x')^2 - c^2t^2)^{3/4}} \tag{29}$$

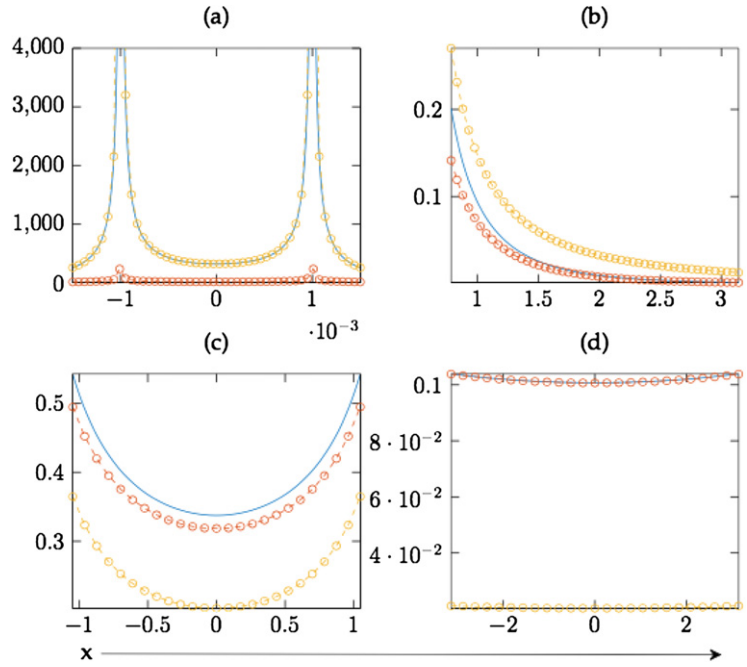

Figure B.1. The exact positive energy Klein–Gordon propagator (25) (blue line), the light cone approximation equation (28) (yellow line) and the WKB approximation (29) (orange line) for (a) $t = 0.001$ and $-0.0015 \leqslant x \leqslant +0.0015$; (b) $t = \pi/8$ and $\pi/4 \leqslant x \leqslant \pi$; (c) $t = \pi/2$ and $-\pi/3 \leqslant x \leqslant \pi/3$; (d) $t = 5\pi$ and $-\text{pi} \leqslant x \leqslant \pi$. We have used $x' = 0$ and $m = \hbar = c = 1$.

Unlike the light cone approximation, this approach has the unphysical property that the propagator does not become $\delta(x')$ in the limit $(x - x', t) \to (0, 0)$. The Klein–Gordon propagator shares this disagreement between the light cone limit and the large argument limit with some curved space propagators [32]. Even if Nc is not particularly large this approximation is still a good one when $x - x' \gg ct$, so it can provide insight into the acausal contributions to the wavefunction. Once we have made approximations to the propagator it is important to demonstrate how good they are. To this end we show in figure B.1 the exact propagator and both the light cone and the saddle point approximations to it for a series of values of x and t. We can deduce from this that at all times apart from very close to $t = 0$ the saddle point approximation is better than the light cone approximation.

C. The saddle–pole approximation

The above two sections treat the saddle points and poles separately. This is correct if the saddles and poles are far apart. However that may not always be the case. If they do become close to one another it is not correct to treat them separately. The saddle and pole are said to coalesce when this occurs. Indeed, for our case figure 6 shows the saddle point x_2 and the pole at $x' = x + ct$ may well coalesce. This is difficult to deal with because the approximations are not equal at the pole, the saddle point approximation has a singularity at this point while the light cone approximation has a simple pole. Therefore we need a new approximation. To obtain a suitable propagator for this case we employ a Mellin–Barnes representation of the modified Bessel function [31]

$$K_1\left(Nc\sqrt{(x-x')^2-c^2t^2}\right) = \frac{\mathrm{i}}{2\pi^2}\left(\frac{\pi}{2Nc\sqrt{(x-x')^2-c^2t^2}}\right)^{1/2} \times \exp\left(-Nc\sqrt{(x-x')^2-c^2t^2}\right)\int_{-\mathrm{i}\infty}^{\mathrm{i}\infty}\Gamma(\tau)\Gamma\left(-\tau-\frac{1}{2}\right) \times \Gamma\left(\frac{3}{2}-\tau\right)\left(2Nc\sqrt{(x-x')^2-c^2t^2}\right)^{\tau}\mathrm{d}\tau \tag{30}$$

Substituting this into equation (25) gives

$$\triangle_{\pm}(x',x,t) = \mp\frac{Nc^2t}{2\pi^3}\left(\frac{\pi}{2Nc\sqrt{(x-x')^2-c^2t^2}}\right)^{1/2}\frac{\exp\left(-Nc\sqrt{(x-x')^2-c^2t^2}\right)}{\sqrt{(x-x')^2-c^2t^2}} \times \int_{-\mathrm{i}\infty}^{\mathrm{i}\infty}\Gamma(\tau)\Gamma\left(-\tau-\frac{1}{2}\right)\Gamma\left(\frac{3}{2}-\tau\right)\left(2Nc\sqrt{(x-x')^2-c^2t^2}\right)^{\tau}\mathrm{d}\tau \tag{31}$$

We see that the pre-factor here looks very similar to the propagator in the saddle point approximation. The integral in equation (31) can be done by rearranging equation (30). Then using equation (27) for the Bessel function leads to the same expression as we found in the light cone approximation. However in this limit the exponent tends to zero so the exponential can be approximated by unity.

Therefore, in order to have a propagator that is valid when the saddle point and pole coalesce we keep the prefactor as it is but evaluate the integral in the light-cone approximation. Making use of equation (27) a little algebra yields

$$\triangle_{\pm}(x',x;t) = \mp\frac{\mathrm{i}ct}{\pi}\frac{1}{(x-x')^2-c^2t^2}\exp\left(-Nc\sqrt{(x-x')^2-c^2t^2}\right) \tag{32}$$

This approximation has the desired properties. As we take the light-cone limit it behaves as a simple pole, whereas moving away from this into the saddle point regime, the exponential takes over. Equation (32) also yields a δ-function as $(x-x',t)\to(0,0)$. This expression was obtained as an approximation and it is important to investigate the precision and range of validity of this. In figure C.1 we look at the accuracy of the saddle–pole approximation. As expected this expression does provide improved accuracy when the saddle and pole are very close, but the overall effect can be regarded as small.

In figure C.1 we look at the accuracy of the saddle–pole approximation. As expected this expression does provide improved accuracy when the saddle and pole are very close, but the overall effect can be regarded as small.

D. The non-relativistic propagator

In this paper we frequently refer to the non-relativistic limit to relate this work to earlier results. Therefore, for completeness, we examine the non-relativistic limit of equation (25). In this limit $c\to\infty$, and the argument of the modified Bessel function becomes large. This means we can use equation (10.25.3) of reference [31] to approximate the Bessel function as

$$K_1(Nc\sqrt{(x-x')^2-c^2t^2}) = \sqrt{\frac{\pi}{2Nc\sqrt{(x-x')^2-c^2t^2}}}\exp(-Nc\sqrt{(x-x')^2-c^2t^2})$$

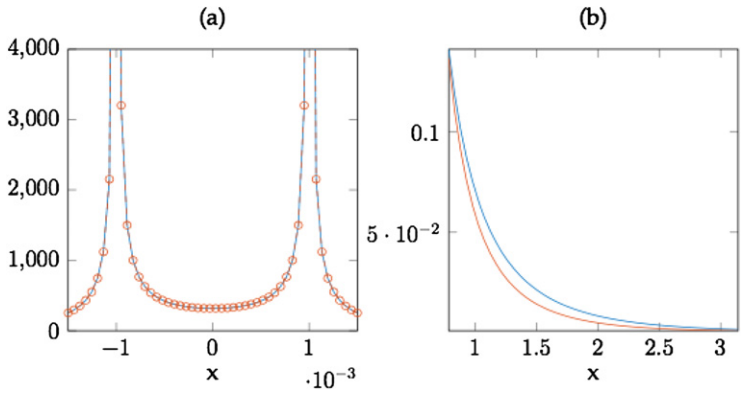

Figure C.1. (a) The exact positive energy Klein–Gordon propagator (25) (blue line), the saddle–pole approximation equation (32) (orange circles) for $t = 0.001$ and $-0.0015 \leqslant x \leqslant +0.0015$; (b) the saddle point approximation (29) and the saddle–pole approximation (32) to the propagator for $t = \pi/8$ and $\pi/4 \leqslant x \leqslant \pi$.

In this limit we can also write

$$\sqrt{(x-x')^2 - c^2t^2} \approx \mathrm{i}ct\left(1 - \frac{(x-x')^2}{2c^2t^2}\right) \tag{33}$$

Putting this into equation (25) and multiplying out the denominator inside the square root gives two terms: $2\mathrm{i}mc^2t$ and $m(x-x')^2/\mathrm{i}t$. At any time greater than zero the first term dominates so we can neglect the second. We also make approximation (33) in the exponent but do not neglect terms there because we are interested in the phase in this work.

$$\triangle_+(x-x',t) \approx \left(\frac{N}{2\pi\mathrm{i}t}\right)\mathrm{e}^{\mathrm{i}N(x-x')^2/(2t)}\mathrm{e}^{-\mathrm{i}Nc^2t} \tag{34}$$

This is the familiar Schrodinger free particle propagator with the extra rest mass term in the phase of the wavefunction in the second exponential as expected.

ORCID iDs

P Strange https://orcid.org/0000-0001-5818-8032

References

[1] di Francia G T 1952 *Nuovo Cim.* **9** 426–38
[2] Aharonov Y, Albert D Z and Vaidman L 1988 *Phys. Rev. Lett.* **60** 1351–4
[3] Berry M V 1994 Faster than Fourier in quantum coherence and reality *Celebration of the 60th Birthday of Yakir Aharonov'* ed J S Anandan and J L Safko (Singapore: World Scientific) pp 55–65
[4] Aharonov Y, Colombo F, Sabadini I, Struppa D C and Tollaksen J 2011 *J. Phys. A: Math. Theor.* **44** 365304
[5] Kempf A and Ferreira P J S G 2004 *J. Phys. A: Math. Gen.* **37** 12067–76
[6] Tollaksen J 2007 *J. Phys.: Conf. Ser.* **70** 012016
[7] Berry M V and Moiseyev N 2014 *J. Phys. A: Math. Theor.* **47** 315203

[8] Katsav E, Perlsman E and Schwartz M 2017 *J. Phys. A: Math. Theor.* **50** 025001
[9] Berry M V and Dennis M R 2009 *J. Phys. A: Math. Theor.* **42** 022003
[10] Berry M V and Fishman S 2018 *J. Phys. A: Math. Theor.* **51** 025205
[11] Berry M V 2013 Superoscillations, endfire and supergain *Quantum Theory: A Two-Time Success Story; Yakir Aharonov Festschrift* ed D Struppa and J Tollaksen (Berlin: Springer) pp 327–36
[12] Berry M V 2016 *Milan J. Math.* **84** 217–30
[13] Dennis M R, Hamilton A C and Courtial J 2008 *Opt. Lett.* **33** 2976–8
[14] Aharonov Y, Colombo F, Sabadini I, Struppa D C and Tollaksen J 2011 *J. Phys. A: Math. Theor.* **50** 185201
[15] Berry M V 2013 *J. Phys. A: Math. Theor.* **46** 205203
[16] Roy T, Rogers E T F and Zheludev N I 2013 *Opt. Express* **21** 7577–80
[17] Rogers E T F, Lindberg J, Roy T, Savo S, Chad J E, Dennis M R and Zheludev N I 2012 *Nat. Mater.* **11** 432–5
[18] Gazit S, Szameit A, Eldar Y and Segev M 2009 *Opt. Express* **17** 23920–46
Gazit S, Szameit A, Eldar Y and Segev M 2009 *Opt. Express* **18** 26631 (Engl. Transl.)
[19] Shechtman Y, Gazit S, Szameit A, Eldar Y and Segev M 2010 *Opt. Lett.* **35** 1148–50
[20] Yuan G H, Vezzoli S, Aluzarra C, Rogers E T F, Couteau C, Soci C and Zheludev N I 2016 *Nat. Light: Sci. Appl.* **5** e16127
[21] Berry M V *et al* 2019 *J. Opt.* **21** 053002
[22] Chen G, Wen Z and Qiu C 2019 *Nat. Light: Sci. Appl.* **8** 56
[23] Berry M V and Popescu S 2006 *J. Phys. A: Math. Gen.* **39** 6965–77
[24] Buniy R V, Colombo F, Sabadini I and Struppa D C 2014 *J. Math. Phys.* **55** 113511
[25] Bussell M and Strange P 2015 *Eur. J. Phys.* **36** 065028
[26] Colombo F, Gantner J and Struppa D C 2017 *J. Math. Phys.* **58** 092103
[27] Strange P 1998 *Relativistic Quantum Mechanics with Applications in Condensed Matter and Atomic Physics* (Cambridge: Cambridge University Press)
[28] Thaller B 1992 *The Dirac Equation* (Berlin: Springer)
[29] Copson E T 2005 *Asymptotic Expansions* (Cambridge: Cambridge University Press)
[30] de Bruijn N G 1981 *Asymptotic Methods in Analysis* (New York: Dover)
[31] NIST 2010 *NIST Handbook of Mathematical Functions* (Cambridge: Cambridge University Press) http://dlmf.nist.gov
[32] Schulman L S 1981 *Techniques and Applications of Path Integration* (New York: Wiley)
[33] Bialynicki-Birula I and Bialynicki-Birula Z 2017 *Phys. Rev. Lett.* **60** 114801
[34] Berry M V 2012 *Eur. J. Phys.* **33** 279